Moisture Diffusion Inside the BEOL of an FC-PBGA Package

Quentin Vandier, Hélène Frémont, and Dominique Drouin, *Member, IEEE*

***Abstract*— Moisture diffusion into the back-end-of-line (BEOL) can be critical for the reliability of electronic devices. With the objective of studying moisture diffusion into critical areas, such as the silicon–organic substrate interfaces of a flip chip plastic ball grid array (FC-PBGA), a multitude of impedance sensors sensitive to moisture are integrated inside the BEOL of a 17 × 17 mm silicon die. The sensors are read by a dedicated custom circuit that allows accurate characterization of the moisture with in situ spatial measurements. This article presents the results obtained by the experimental acquisition system on the FC-PBGA module under a high-relative humidity (RH) level of up to 75%. This study shows the moisture behavior of the multiwalled carbon nanotube (MWCNT) sensors inside the BEOL during absorption and desorption. The behavior initially follows Fick's law, with a constant increase in the RH. For long-term tests of more than 400 h, an asymptotic behavior is observed; when the concentration of a sensor reaches a value close to saturation, a two-dimensional finite-difference method (2D FDM) is used to estimate the saturation value. Thanks to the large number of sensors distributed on the BEOL, we first detect, during an absorption test, an increase in the RH. This increase is due, first of all, to a lateral moisture front with a constant velocity of about 90 μm/h moving through the underfill. Then, after 30 h of storage, a more complex diffusion through the organic substrate occurs, affecting the BEOL.**

***Index Terms*— Flip chip plastic ball grid array (FC-PBGA), long-term high-humidity storage, moisture diffusion, relative humidity (RH) sensors.**

I. Introduction

IN ORDER to fulfill the growing need, increasing at a fast pace, for data processing, storage, and transmission, the industry is developing very large-scale integration (VLSI) systems with an increasing number of active components. In an assembly, this results in an increase in the amount of input–output (I/O) through higher interconnection densities on larger silicon dies and smaller interconnection sizes. However, the increase in the interconnection density, which improves performance, has led to an increase in the vulnerability of the interconnection area inside flip-chip packages. The main sources of failure within the interconnection area are exposure to moisture and temperature excursions. It was reported that moisture induces mechanical stresses, hygroswelling [1], and local pressure variation, which cause delamination and fractures in the interconnections. Further studies have indicated corrosion phenomena [2], [3] and induced galvanic migration, which creates dendrites between the metal coating of the interconnections [4].

For this study, experimental in situ sensors and a custom readout system are developed to follow moisture diffusion inside a flip-chip plastic ball grid array (FC-PBGA) module. This article describes the moisture absorption and desorption of multiwalled carbon nanotubes (MWCNTs)/polyimide sensors inside the back-end-of-line (BEOL) under different environmental conditions and moisture diffusion through an FC-PBGA package.

Manuscript received 24 November 2022; accepted 25 November 2022. Date of publication 1 December 2022; date of current version 27 December 2022. This work was supported by the Natural Sciences and Engineering Research Council of Canada (NSERC) /IBM Industrial Research Chair in High-Performance Heterogeneous Integration. Recommended for publication by Associate Editor A. Chandra upon evaluation of reviewers' comments. *(Corresponding author: Quentin Vandier.)*

Quentin Vandier and Dominique Drouin are with the Institut Interdisciplinaire d'Innovation Technologique (3IT), and the Nanotechnologies and Nanosystems Laboratory (LN2), CNRS UMI-3463, Universite de Sherbrooke, Sherbrooke, QC J1K 0A5, Canada (e-mail: quentin.vandier@usherbrooke.ca).

Hélène Frémont is with the Laboratoire de l'Intégration du Matériau au Système, CNRS UMR 5218, Universite de Bordeaux, 33400 Talence, France.

Color versions of one or more figures in this article are available at https://doi.org/10.1109/TCPMT.2022.3226139.

Digital Object Identifier 10.1109/TCPMT.2022.3226139

II. Method

A. Integrated Sensors

The embedded sensor is composed of MWCNTs functionalized with carboxyl groups (COOH-MWCNTs). The sensors located in the BEOL are fabricated by depositing functionalized MWCNTs with a spray coating method; they are then patterned with UV photolithography to achieve a rectangular form that is 20 μm in length and 100 μm in width. They are electrically isolated by polyimide, which allows moisture to diffuse into the MWCNTs [5].

The MWCNTs' sensors have a complex sensing mechanism due to the different interconnections between MWCNTs and water molecules. The frequency response of the sensors follows an R/C model. The temperature and moisture concentration modify the equivalent resistance and capacitance. The sensing mechanism was studied in a previous work by Quelennec et al. [6] and its sensitivity (S_Z) to temperature (T) and relative humidity (RH) were reported to vary with different frequencies according to (1) [6]. The moisture concentration inside each sensor can be extracted using its impedance variation (RV) from an impedance reference (Z_{ref}) at a fixed frequency, as described by (2) [7]

$$Z = Z_{\text{ref}}\big(1 + s_{Z,T}(f)(T - T_{\text{ref}}) + s_{Z,\text{RH}}(f)(\text{RH} - \text{RH}_{\text{ref}})\big) \quad (1)$$

$$\text{RV}(f) = \frac{|Z(f)| - |Z_{\text{ref}}(f)|}{|Z_{\text{ref}}(f)|}. \quad (2)$$

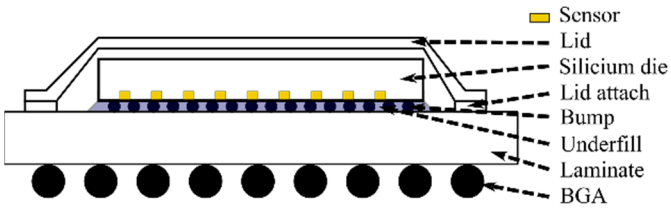

Fig. 1. Representative schematic of the FC-PBGA module with sensors (yellow blocks) embedded in the BEOL.

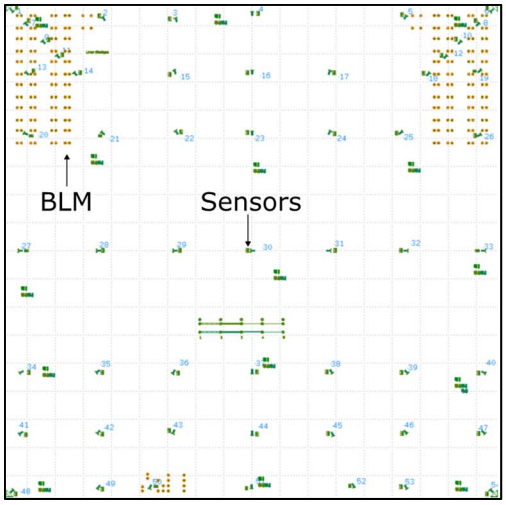

Fig. 2. Sensors (green pattern with ID numbers) and BLM (orange circle) positions shown on the silicon chip layout.

The sensors are sensing at 10 kHz, which is high enough to allow the lock-in amplifier to eliminate most of the flicker noise. Furthermore, the stated frequency is also sufficiently far away from the sensors' cutoff frequency, allowing a high RH sensitivity.

B. Sensor Module

In each 17 × 17 mm silicon chip, 108 carbon nanotube (CNT) sensors are embedded, covering the entire silicon die area. The silicon die is assembled into FC-PBGA modules on a 0.856-mm high Tg with a base core of 0.400-mm glass epoxy laminate and ten Cu layers (see Fig. 1). The different locations of the sensor and their interconnections with the substrate [ball limiting metallurgy (BLM)] shown in Fig. 2 allow to analyze moisture at a particular location inside the module but also to monitor the diffusion vectors from the edge to the center of the die. In order to read the sensors, a lock-in amplifier has been designed and implemented on a distant printed circuit board (PCB) [8]. Each FC-PBGA module is mounted on a flexible board that allows the ball grid array (BGA) to be connected to the readout circuit outside the Thermotron SM-16-7800 environmental chamber. The environmental chamber provides accurate temperature and RH values for the characterization of the sensor's modules (see Fig. 3).

III. Characterization of Experimental Sensors

A few modules are assembled without underfill and wired to the readout system via the flip-chip interconnection to

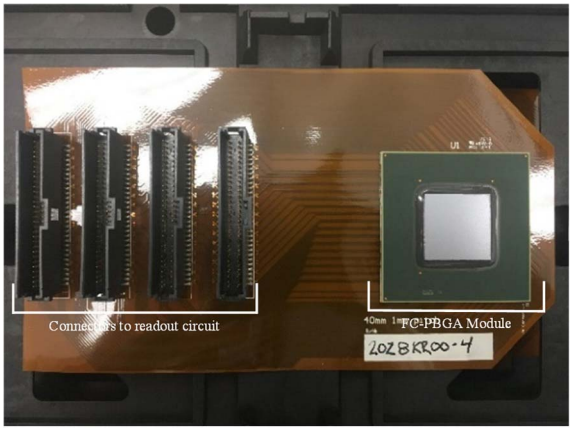

Fig. 3. FC-PBGA module (on the right side) without lids assembled by the BGA on flexible PCB with four readout connectors (on the left side).

ensure a direct exposure of the BEOL to the ambient humidity. This module enables the calibration and characterization of all integrated sensors on a silicon chip.

Fig. 4 shows measurements made with the sensors during an absorption with two steps of 75% RH and 85% RH and initially dry conditions. All sensors detect the increase in the moisture concentration simultaneously and without any delay. The moisture saturation level is reached after about 10 h, as shown in Fig. 4, during the first 75% RH step. For desorption, the same absence of a delay is observed. The embedded sensors are sensitive to moisture and temperature, with a linear behavior from 30 °C to 130 °C and from 30% RH to 75% RH. All the measurements made during the characterization of the sensors with a dedicated readout system show, for the sensors with a dedicated readout system, measurement uncertainties of 0.6 °C and 0.2% RH. This performance is achieved with sensors with a sensitivity of 0.3% RV/% RH and a lock-in amplifier with an uncertainty of 0.1% RV. A nonlinear behavior due to the sensors appears at 85% RH, as shown in Fig. 4, during the second moisture step that occurs at 19 h; this is probably caused by a degradation of the sensors or interconnections. In order to avoid this issue, we stay within the working range of our sensors: we limit the RH level inside the chamber to 75%.

The no-underfill test demonstrates the need for a desorption process after storage in a high-moisture environment in order to dry the BEOL. In some packages, residual moisture is detected after a long-duration high-moisture test. A higher temperature (>100 °C) is required to remove the residual bound water [9], [10]. Dai et al. [11] described this residual bound water as being mostly localized inside the substrate; hence, most of it is not detected by the sensors located within the BEOL. A standard duration of 24 h at 130 °C completely dries the BEOL of an FC-PBGA module without underfill; it also demonstrates the robustness of the sensors after multiple measurements.

IV. Humidity Absorption

FC-PBGA sensors with underfill were used for the study of moisture diffusion in a typical assembly module. As illustrated

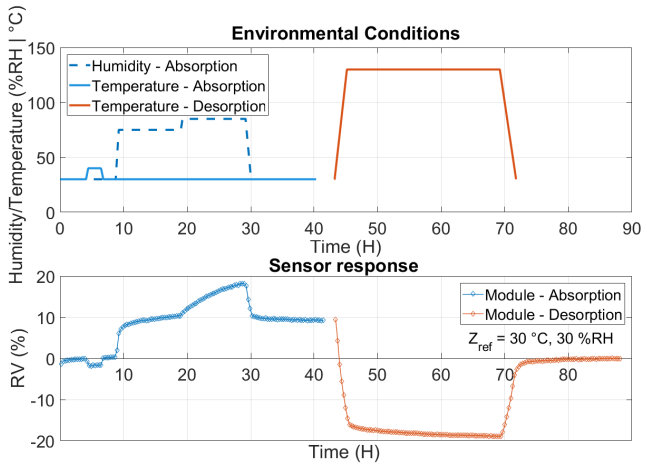

Fig. 4. Module-without-underfill sensor's response to temperature and humidity variation with 75% RH and 85% RH steps inside the environmental chamber and desorption at 130 °C during baking. Top: RH (% RH) and temperature (°C) of the environmental chamber. Bottom: relative impedance variation of the sensor (%).

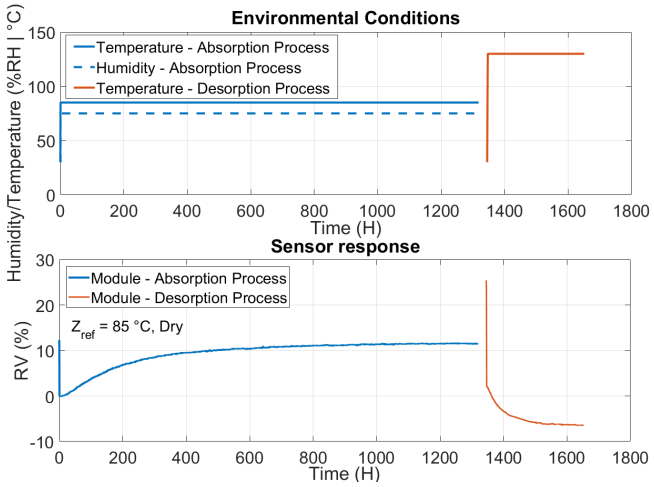

Fig. 5. Example of a sensor's response inside a module with underfill to absorption in the environmental chamber (blue) and desorption during baking (red). Top: RH (% RH) and temperature (°C) of the environmental chamber. Bottom: relative impedance variation of the sensor (%).

in Fig. 5, with an RH of 75%, the absorption process consists of 1300 h of constant moisture exposure in the environmental chamber at a fixed temperature of 85 °C in order to accelerate the diffusion inside the underfill. Before and after each absorption process, the module is dried at 130 °C for 250 h.

During this experiment, three observations have been made. The behavior of integrated sensors to the absorption of humidity by the package (see Section IV-A). The variation of the RH inside the sensor according to their position (see Section IV-B). The evolution of the moisture fronts according to the absorption time to monitor the diffusion vector (see Section IV-C).

A. Single Sensor Behavior

The local moisture diffusion of each individual sensor of the assembled die shows behavior in agreement with the expected

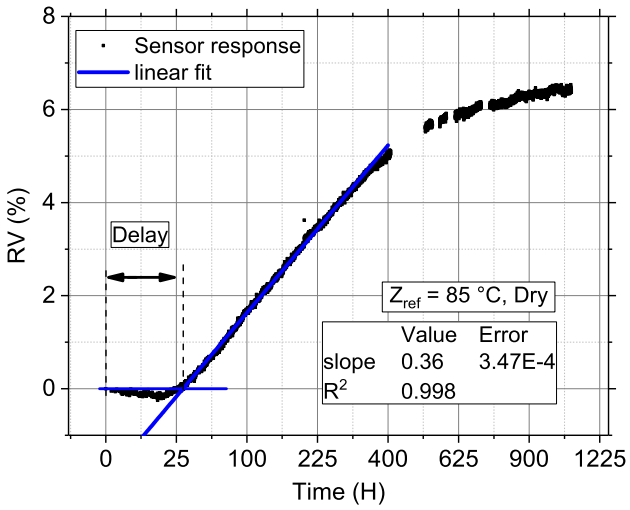

Fig. 6. Individual sensor's response in terms of the relative impedance variation (%) to the absorption of humidity with a 75% ambient humidity level. A linear fit of the data from 50 to 250 h is displayed.

Fickian response, with a linear rise of the relative impedance followed by a curvature to a saturation state (see Fig. 6). Compared to the test without underfill, the sensor's response shows a delay that indicates the impervious properties of the underfill. This information was used to track the humidity vector inside the package (see Section IV-C).

This Fickian behavior is expected, as observed in many epoxy/polymer moisture uptake experiments with weight measure [12], [13]; however, non-Fickian behavior has also been observed in the literature, especially in high-temperature environments, where a dual-stage diffusion model is used [14], [15], [16], [17], [18], [19]. The moisture saturation concentration (C_{sat}) that is obtained when the impedance of the sensors is stabilized is related to the ambient RH set by the environmental chamber, the solubility (S), and the saturated vapor pressure ($P_{v,\text{sat}}$). The concentration is linearly proportional to a factor M (modified solubility) multiplied by the ambient RH at a constant temperature, as shown in (3) [20], [21]. The moisture saturation concentration is proportional to the maximum relative impedance (RV_{sat}) observed and can be determined, thanks to the sensitivity of the sensors toward moisture (s_{RH}) (4). The characterization of the sensors without underfill shows a linear response of RH in a range of 0% RH–75% RH (see Section III) which permit to identify in a constant temperature environment with known RV_{sat}, the RH and moisture concentration inside different sensors with different s_{RH}

$$C_{\text{sat}} = S \times \text{RH} \times P_{v,\text{sat}} = M \times \text{RH} \tag{3}$$

$$\text{RV}_{\text{sat}} = C_{\text{sat}} \times s_{\text{RH}}. \tag{4}$$

The test performed with the sensor module inside the environmental chamber for 1300 h allows one to observe the linear behavior of the moisture concentration versus the square root of time, followed by a curvature toward a saturation level. In order to estimate the saturation time due to the asymptotic behavior observed during long-term storage, a diffusion model, obtained using an analogy between the well-known

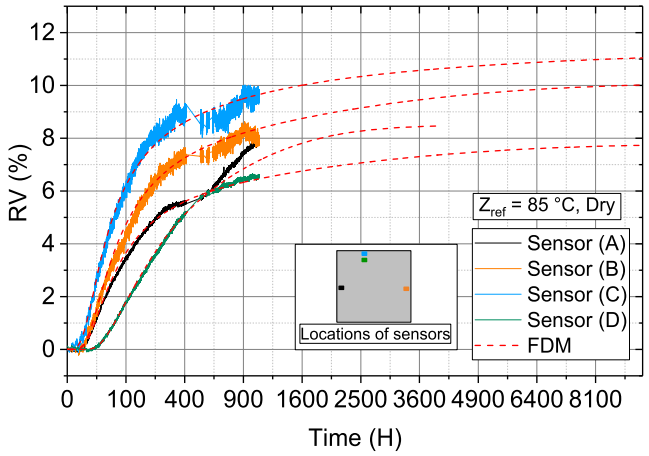

Fig. 7. Four sensors' responses in terms of the relative impedance variation (%) over 1300 h (continuous lines) and the corresponding 2D-FDM models (dashed lines) during moisture diffusion with initially dry modules.

TABLE I

VALUES OF THE DIFFUSION COEFFICIENT (D) AND EQUIVALENT IMPEDANCE OF MOISTURE SATURATION INSIDE SENSORS (RV_{sat}) ESTIMATED USING 2D FDM AND THE SENSORS' RESPONSES TO MOISTURE ABSORPTION AT 75% RH OVER 1300 H

Sensor ID	D (m^2/s)	RV_{sat} (% RV)
(A)	$1.5*10^{-12}$	7.8
(B)	$1.5*10^{-12}$	10.1
(C)	$1*10^{-12}$	11.2
(D)	$5.5*10^{-12}$	8.5

thermal diffusion equation and moisture diffusion, was used [20], [22], [23].

B. Moisture Absorption Inside BEOL

The spatial distribution of the sensor inside the BEOL allows to have an analysis of the lateral moisture diffusion. A 2-D finite-difference method (FDM) is used along with the sensor response over 1300 h (see Fig. 7) to estimate the saturation impedance value of the sensors (RV_{sat}) as well as the diffusion coefficient (D) despite the variation of the sensitivity between sensors. This FDM model using the Fickian equation is commonly used for moisture diffusion inside materials such as IC materials, it allows to extract a diffusion coefficient in order to relate the diffusion to the sensor's position [24], [25]. The diffusion coefficient calculated by the FDM has the same values for sensors located equidistantly from the edge of the silicon die, such as sensors A and B [see Fig. 7 (inset)]. The diffusion coefficient is estimated to be between 0.8×10^{12} and 3×10^{12} m^2/s for sensors near the die edge (sensor C). For sensors at the border of the die, the measured diffusion coefficient extracted from the 2D-FDM shows similar values. For sensors located closer to the center of the die, we have

TABLE II

PARAMETERS OF LINEAR FIT TO THE DELAY OF SENSORS FROM 0 TO 3500 μM

45% RH		60% RH		75% RH	
Slope	Error	Slope	Error	Slope	Error
86.5	3.6	129	11.7	95	3.9

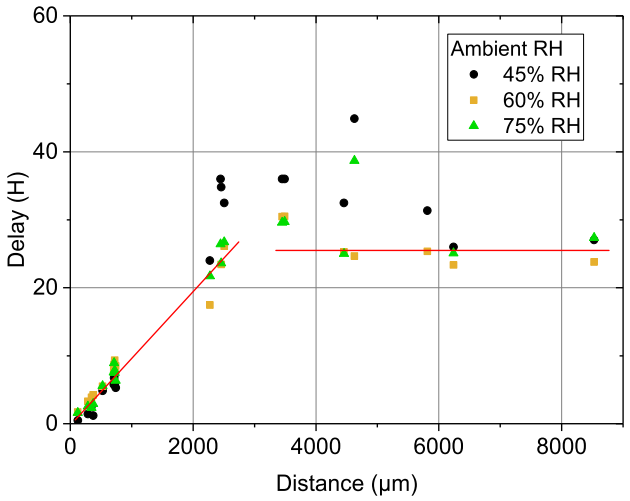

Fig. 8. Moisture front inside the underfill visible through the sensor's moisture detection delay versus the distance of the sensors from the edge of the die at different ambient moisture levels (45% RH, 60% RH, and 75% RH).

higher diffusion coefficients, as shown by sensor D in Table I. We did not perform these calculations for sensors close to the center (~3500 μm) of the die because the FDM could not be used to successfully calculate diffusion coefficients for these sensors. This phenomenon can be explained by a second diffusion path that does not come from the die edge. In order to have a more accurate estimation of the RH at the die center, a 3-D diffusion model with two different diffusion coefficients is required. As seen in Fig. 7, a few sensors, such as sensor A, show a non-Fickian behavior with two-stage saturation. This behavior has also been observed in epoxy used as underfill during long-term moisture absorption [10].

C. Moisture Propagation Front

Unlike the module without underfill described in Section III, each sensor has a response delay, as shown in Fig. 5, between 0 and 30 h before the impedance increase due to moisture absorption inside the CNT sensors takes place. As can be seen in Fig. 8, the delay before moisture detection by the sensors has a linear evolution related to the distance from the sensors to the edge of the silicon die for distances <3500 μm. A linear fit provides an estimation of the moisture velocity (see Table II). This proportional evolution supports a lateral moisture front penetrating through the underfill to the sensors with a constant speed of ~90 μm/h (see Fig. 9). For the sensors at distances >3500 μm, we can see that the response delays are similar and not a function of the position anymore. As previously observed for the diffusion

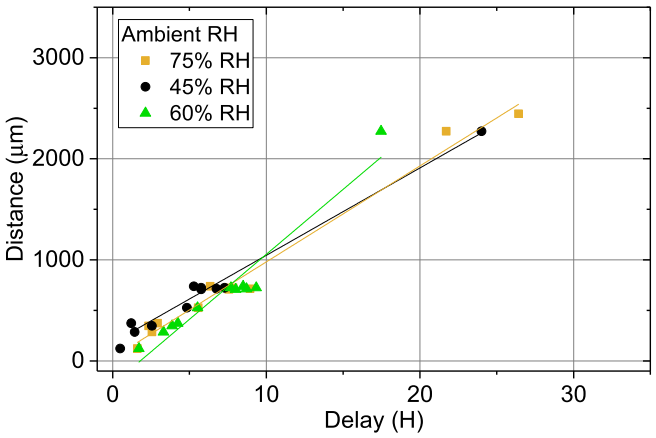

Fig. 9. Distances of the sensors from the edge compared to their delays at different ambient RHs (45%, 60%, and 75%). The moisture front penetration speed through the underfill is extracted from the sensors' data.

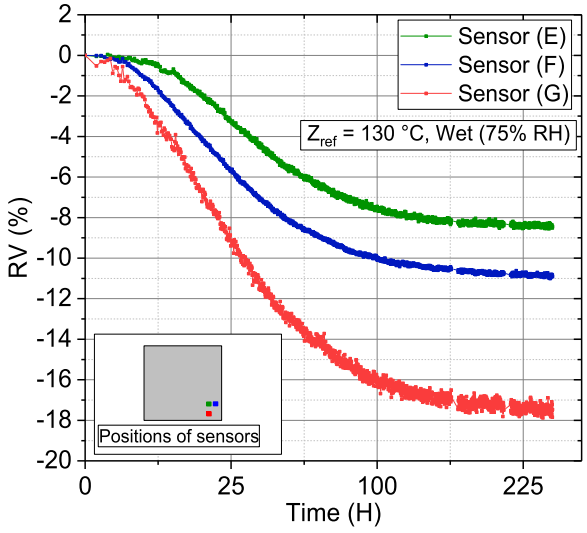

Fig. 10. Three sensors' responses in terms of the relative impedance variation (%) to a desorption process over 250 h at 130 °C with an initial moisture level of 75% RH.

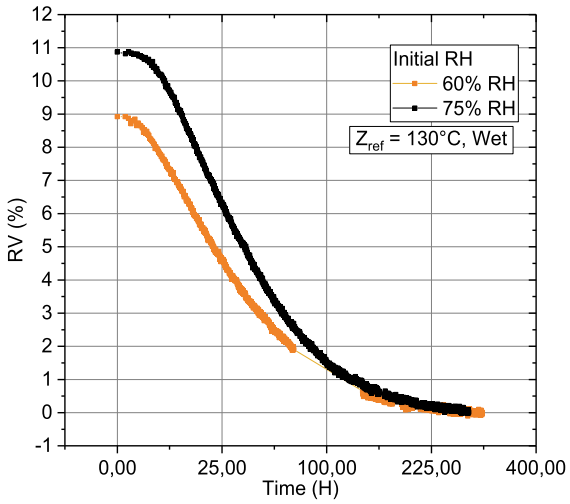

Fig. 11. Desorption response in terms of the relative impedance variation (%) of the same sensor inside the BEOL during a bake at 130 °C with initial moisture levels of 60% RH and 75% RH.

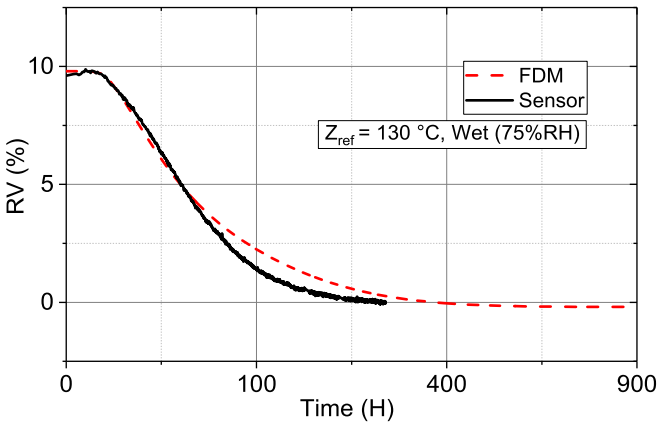

Fig. 12. Sensor's response in terms of the relative impedance variation (%) to a desorption process (continuous line) and the 2D-FDM model estimate of the sensor's response (dashed line) with Z_{ref} at 130 °C and an initial state of 75% RH.

coefficient calculated using the FDM in Section IV-B, this behavior can be explained by a vertical moisture front moving through the organic substrate. This second moisture front will affect the die BEOL after about 30 h of moisture exposure regardless of the humidity levels in the environment (45% RH–75% RH), this would indicate a moisture propagation rate of 28 μm/h through the laminate. In the literature study of moisture absorption in fiber glass, the substrate has been done by weight measurement [26]. However, the impact of metallic lines and ground plane on the moisture diffusion with local moisture uptake measurement must be taken into consideration in order to have an accurate study of the moisture vector through the laminate.

V. Humidity Desorption

The sensor module was also used to study the desorption of moisture inside the die BEOL during a desorption process in a controlled atmosphere using nitrogen flow. Unlike in the module without underfill, the standard 24-h desorption process at 130 °C is not enough to achieve a dry equilibrium. The responses of three sensors to an extended desorption process that continues for 250 h to reach a dry state are shown in Fig. 10 after an absorption process at 75% RV over 1500 h. The same Fickian behavior seen in the response during absorption is observed for all sensors. Different initial moisture levels have no influence on the time constant of the desorption curve, as shown in Fig. 11. Hence, the dynamics are independent of the initial moisture and a unique 250-h bake duration is required to completely dry the module after storage at any moisture and temporal conditions.

After 250 h, the sensors seem to have reached their dry state (see Fig. 12). An asymptotic behavior is visible starting at 216 h (99% of the dry ratio). The moisture desorption for each sensor can be plotted as the ratio of RV over RV_{sat} that is extracted from the 2-D model (dry sensors) as a function of the distance of the sensor from the die edge (see Fig. 13). We can observe from this data that the desorption in the

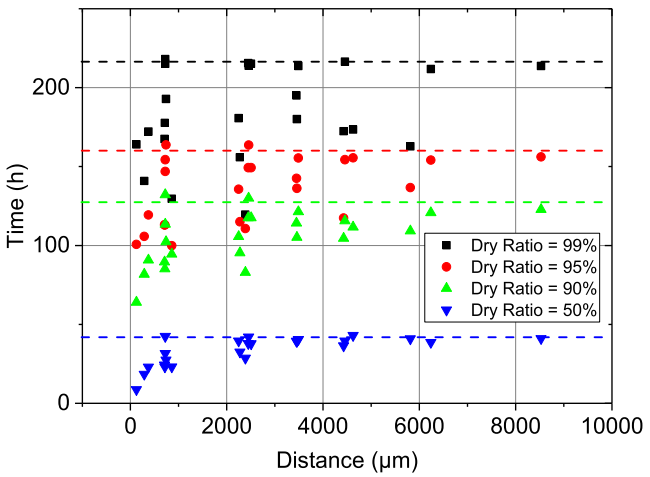

Fig. 13. Evolution of time (h) needed to achieve the $RVRV_{sat}$ (dry) ratios 50%, 90%, 95%, and 99% for each sensor inside an FC-PBGA module during a desorption process at 130 °C with an initial state of 75% RH.

module is not uniform near the edge of the die. For the first ~1000 μm from the edge, a gradual drying time is measured depending on the sensor position. Similar nonlinear behavior was also observed during the absorption (see Section IV-C). This increasing drying time is not observed for sensors located farther than 1000 μm from the edge, where there is a plateau that probably indicates a second path for moisture desorption.

VI. Conclusion

The experimental setup with CNT sensors integrated inside the BEOL of an FC-PBGA allows an accurate local moisture value to be obtained during humid storage for more than 1300 h. The complete set of measuring instruments achieves a measurement accuracy of 0.2% RH on each of the 54 in situ sensors spread over the 17 × 17 mm silicon die.

When the ambient RH increases during the absorption test, all individual sensors respond with an increase in the impedance. This increase in the impedance shows a Fickian behavior of moisture diffusion and an asymptotic behavior when the sensors have a moisture concentration approaching their saturation state at a fixed RH. This behavior appears after 400–900 h depending on the position of the sensor in the die. As the humidity saturation level is not fully obtained inside the module after 1300 h of moisture exposure, a 2-D finite-difference model with diffusion mainly propagating through the underfill is used to calculate the saturation time, which is estimated to be 9000 h. This simulation also allows one to estimate the diffusion coefficient of the moisture inside the BEOL. During the desorption test, the same Fickian behavior is visible for around 250 h at 130 °C under nitrogen. Using the FDM, the 99% desorption level is estimated at ~216 h and the completely dry state is estimated at ~900 h. Similar diffusion coefficients were measured on sensors near the die edge. The estimated coefficients from the FDM are more variable for the sensors near the die center, which shows the limit of the model used.

The diffusion of humidity from the edge of the die to the center can be followed by examining the variation in the delay between the detection of moisture for each sensor and the increase in the chamber humidity. This behavior indicates a constant speed of the moisture front for the first 3500 μm from the edge of the die. From 4000 to 8000 μm, the moisture front propagation is not visible anymore, as similar response delays of 30 h are measured. This can be explained by the major impact of significant vertical moisture diffusion through the organic laminate on the central sensors. This assumption supports the coefficients calculated with the 2D-FDM; a different diffusion happens in the center of the BEOL (more than 3500 μm from the edge). This work could be improved by a more accurate 3-D finite-element analysis. This would demonstrate the importance of a vertical moisture front moving through the organic laminate and its impact on different locations inside the BEOL. The custom setup shows that it is possible to follow the moisture level locally inside the BEOL. The impact of filler materials has not been investigated as this underfill is part of our partner assembly process of the record. The proposed sensors technology could be applied to characterize the moisture diffusion through different filler content. With an integrated version of this circuit, a full embedded acquisition chain can be realized to monitor moisture and temperature levels to prevent the dysfunction of the microelectronic system through interconnection failure.

TABLE III
Analogy Between Thermal Diffusion and Moisture Diffusion

	Thermal	Direct	Normalized	Advanced
Variable	T (K)	C (kg/m^3)	φ ($kg.P_a/m^3$)	Φ (%RH)
Conductivity	K (W/mK)	D (m^2/s)	D*S ($kg.m/m^2.s.P_a$)	D*M (kg/m/s)
Materials	ρ C_p ($J/k/m^3$)	1	S ($kg/m^3/Pa$)	M (kg/m^3)
Boundary conditions		C_{sat} (kg/m^3)	P_v (kg/m^3)	RH (%RH)

Appendix

In order to build a 2-D model, we used an analogy, as shown in Table III, between the well-known thermal diffusion process (4) and moisture diffusion (5).

In a homogenous material, the analogy replaced the heat conductivity (K) by a coefficient ($D \times M$) proportional to the diffusion coefficient. This model allows one to determine the lateral diffusion parameters, like the diffusion coefficient (D) and the saturation level of impedance, which is related to the concentration saturation inside the sensor (RV_{sat}).

To perform a 2-D simulation, a finite-difference model implemented in MATLAB[1] is used to simulate diffusion inside the BEOL of the FC-PBGA module (6), using the RV_{sat} value

[1]Registered trademark.

as the saturation value

$$\rho C_p \frac{\partial T}{\partial t} = K\frac{\partial^2 T}{\partial x^2} + K\frac{\partial^2 T}{\partial y^2} \tag{5}$$

$$\frac{\partial C}{\partial t} = D1\frac{\partial^2 C}{\partial x^2} + D2\frac{\partial^2 C}{\partial y^2} \tag{6}$$

$$\Phi_{x,y}^{t+1} = \Phi_{x,y}^{t} + \Delta t * MD * \left[\left(\frac{\Phi_{x-1,y}^{t} - 2\Phi_{x,y}^{t} + \Phi_{x+1,y}^{t}}{(\partial x)^2}\right) + \left(\frac{\Phi_{x,y-1}^{t} - 2\Phi_{x,y}^{t} + \Phi_{x,y+1}^{t}}{(\partial y)^2}\right)\right]. \tag{7}$$

ACKNOWLEDGMENT

Quentin Vandier would like to thank IBM reliability teams who provided their expertise to help with this project. Quentin Vandier, Hélène Frémont, and Dominique Drouin would also like to thank the internship student and postdoctoral student of the Institut Interdisciplinaire d'Innovation Technologique (3IT), Universite de Sherbrooke, Sherbrooke, Canada, who helped with this project.

REFERENCES

[1] Y. He, "In-situ characterization of moisture absorption-desorption and hygroscopic swelling behavior of an underfill material," in *Proc. IEEE 61st Electron. Compon. Technol. Conf. (ECTC)*, May 2011, pp. 375–386, doi: 10.1109/ECTC.2011.5898541.

[2] M. Wang, J. Wang, H. Feng, and W. Ke, "Effect of Ag_3Sn intermetallic compounds on corrosion of $Sn_{-3.0}Ag_{-0.5}Cu$ solder under high-temperature and high-humidity condition," *Corrosion Sci.*, vol. 63, pp. 20–28, Oct. 2012, doi: 10.1016/j.corsci.2012.05.006.

[3] S. S. Ha, H. Kang, G. R. Kim, S. Pae, and H. Lee, "Effect of corrosion on mechanical reliability of Sn-Ag flip-chip solder joint," *Mater. Trans.*, vol. 57, no. 11, pp. 1966–1971, 2016, doi: 10.2320/matertrans.M2016203.

[4] S. J. Krumbein, "Electrolytic models for metallic electromigration failure mechanisms," *IEEE Trans. Rel.*, vol. 44, no. 4, pp. 539–549, Dec. 1995, doi: 10.1109/24.475971.

[5] A. Quelennec, U. Shafique, E. Duchesne, H. Fremont, and D. Drouin, "Smart packaging: A micro-sensor array integrated to a flip-chip package to investigate the effect of humidity in microelectronics package," in *Proc. IEEE 67th Electron. Compon. Technol. Conf. (ECTC)*, May 2017, pp. 513–519, doi: 10.1109/ECTC.2017.140.

[6] A. Quelennec, É. Duchesne, H. Frémont, and D. Drouin, "Source separation using sensor's frequency response: Theory and practice on carbon nanotubes sensors," *Sensors*, vol. 19, no. 15, p. 3389, Aug. 2019, doi: 10.3390/s19153389.

[7] A. Quelennec, Y. Ayadi, Q. Vandier, E. Duchesne, H. Fremont, and D. Drouin, "Smart packaging–microscopic temperature and moisture sensors embedded in a flip-chip package," in *Proc. IEEE 68th Electron. Compon. Technol. Conf. (ECTC)*, May 2018, pp. 1639–1644, doi: 10.1109/ECTC.2018.00247.

[8] Q. Vandier, J. Pezard, H. Fremont, E. Duchesne, and D. et Drouin, "Readout circuit implemented on PCB-level for embedded CNT sensors," in *Proc. IEEE Int. Instrum. Meas. Technol. Conf. (IMTC)*, Dubrovnik, Croatia, May 2020, pp. 1–6, doi: 10.1109/I2MTC43012.2020.9128884.

[9] Y. C. Lin and X. Chen, "Investigation of moisture diffusion in epoxy system: Experiments and molecular dynamics simulations," *Chem. Phys. Lett.*, vol. 412, nos. 4–6, pp. 322–326, Sep. 2005, doi: 10.1016/j.cplett.2005.07.022.

[10] X. Ma, K. M. B. Jansen, L. J. Ernst, W. D. van Driel, O. van der Sluis, and G. Q. Zhang, "Characterization and modeling of moisture absorption of underfill for IC packaging," in *Proc. 8th Int. Conf. Electron. Packag. Technol.*, Aug. 2007, pp. 1–5, doi: 10.1109/ICEPT.2007.4441451.

[11] W. Q. Dai et al., "Study on moisture behavior in flip chip BGA packages and bake process optimization," in *Proc. Int. Conf. Electron. Packag. Technol. High Density Packag.*, Aug. 2009, pp. 1225–1228, doi: 10.1109/ICEPT.2009.5270624.

[12] M.-H. Tsai, F.-J. Hsu, M.-C. Weng, and H.-C. Hsu, "Advanced moisture diffusion model and hygro-thermo-mechanical design for flip chip BGA package," in *Proc. Int. Conf. Electron. Packag. Technol. High Density Packag.*, Aug. 2009, pp. 1002–1008, doi: 10.1109/ICEPT.2009.5270573.

[13] X. J. Fan, S. W. R. Lee, and Q. Han, "Experimental investigations and model study of moisture behaviors in polymeric materials," *Microelectron. Rel.*, vol. 49, no. 8, pp. 861–871, Aug. 2009, doi: 10.1016/j.microrel.2009.03.006.

[14] B. Han and D.-S. Kim, "Moisture ingress, behavior, and prediction inside semiconductor packaging: A review," *J. Electron. Packag.*, vol. 139, no. 1, Mar. 2017, Art. no. 010802, doi: 10.1115/1.4035598.

[15] T. Ferguson and J. Qu, "Moisture absorption analysis of interfacial fracture test specimens composed of no-flow underfill materials," *J. Electron. Packag.*, vol. 125, no. 1, pp. 24–30, Mar. 2003, doi: 10.1115/1.1524132.

[16] H. Frémont, J. Y. Delétage, A. Pintus, and Y. Danto, "Evaluation of the moisture sensitivity of molding compounds of IC's packages," *J. Electron. Packag.*, vol. 123, no. 1, pp. 16–18, Mar. 2001, doi: 10.1115/1.1326436.

[17] H. Park, "Characterization of moisture diffusion into polymeric thin film," *Exp. Mech.*, vol. 53, no. 9, pp. 1693–1703, Nov. 2013, doi: 10.1007/s11340-013-9775-9.

[18] M. R. Vanlandingham, R. F. Eduljee, and J. W. et Gillespie, "Moisture diffusion in epoxy systems," *J. Appl. Polym. Sci.*, vol. 71, no. 5, pp. 787–798, 1999, doi: 10.1002/(SICI)1097-4628(19990131)71:5<787:AID-APP12>3.0.CO.2-A.

[19] M. D. Placette, X. Fan, J.-H. Zhao, and D. Edwards, "Dual stage modeling of moisture absorption and desorption in epoxy mold compounds," *Microelectron. Rel.*, vol. 52, no. 7, pp. 1401–1408, Jul. 2012, doi: 10.1016/j.microrel.2012.03.008.

[20] C. Jang, S. Park, B. Han, and S. Yoon, "Advanced thermal-moisture analogy scheme for anisothermal moisture diffusion problem," *J. Electron. Packag.*, vol. 130, no. 1, pp. 1–8, Mar. 2008, doi: 10.1115/1.2837521.

[21] E. H. Wong, S. W. Koh, K. H. Lee, and R. Rajoo, "Advanced moisture diffusion modeling and characterisation for electronic packaging," in *Proc. 52nd Electron. Compon. Technol. Conf.*, May 2002, pp. 1297–1303, doi: 10.1109/ECTC.2002.1008273.

[22] A. Sasi and P. Gromala, "Simulating moisture diffusion in polymers using thermal-moisture analogy," in *Proc. 17th Int. Conf. Thermal, Mech. Multi-Physics Simul. Experiments Microelectron. Microsystems (EuroSimE)*, Apr. 2016, pp. 1–8, doi: 10.1109/EuroSimE.2016.7463372.

[23] S. Yoon, B. Han, and Z. Wang, "On moisture diffusion modeling using thermal-moisture analogy," *J. Electron. Packag.*, vol. 129, no. 4, pp. 421–426, Dec. 2007, doi: 10.1115/1.2804090.

[24] L. Chen, J. Zhou, H. Chu, and X. Fan, "A unified and versatile model study for moisture diffusion," in *Proc. IEEE 67th Electron. Compon. Technol. Conf. (ECTC)*, May 2017, pp. 1660–1667, doi: 10.1109/ECTC.2017.239.

[25] L. Chen, J. Zhou, H.-W. Chu, G. Zhang, and X. Fan, "Modeling nonlinear moisture diffusion in inhomogeneous media," *Microelectron. Rel.*, vol. 75, pp. 162–170, Aug. 2017, doi: 10.1016/j.microrel.2017.06.055.

[26] Y. He and X. Fan, "In-situ characterization of moisture absorption and desorption in a thin BT core substrate," in *Proc. 57th Electron. Compon. Technol. Conf.*, Sparks, NV, USA, May 2007, pp. 1375–1383, doi: 10.1109/ECTC.2007.373974.

Quentin Vandier received the B.S. and M.S. degrees from the University of Bordeaux 1, Talence, France, in 2014 and 2016, respectively, and the Ph.D. degree from the University of Sherbrooke, Sherbrooke, QC, Canada.

He worked on the design of a readout system that uses embedded sensors inside a microelectronic package for reliability.

Hélène Frémont is currently a Professor with the University of Bordeaux, Talence, France. She is also leading the Packaging, Assembly and Electromagnetic Compatibility (PACE) Team, Integration from the Material to the System (IMS) Laboratory, University of Bordeaux. She has coauthored more than 120 scientific articles, including journal and conference publications, book chapters, and invited articles. Her research expertise is in the fields of microelectronics reliability and failure analysis.

Prof. Frémont is a member of the technical committees of different Component, Packaging and Manufacturing Technology (CPMT)-IEEE conferences and the Organizing Committee of the European Symposium on the Reliability of Electron Devices, Failure Physics and Analysis (ESREF).

Dominique Drouin (Member, IEEE) received the Electrical Engineering degree in 1994 and the Ph.D. degree in mechanical engineering from the University of Sherbrooke, Sherbrooke, QC, Canada, in 1998.

He is the holder of the Natural Sciences and Engineering Research Council of Canada (NSERC)/IBM Industrial Research Chair in high-performance heterogeneous integration and has been a Professor with the Electrical and Computer Engineering Department, University of Sherbrooke, since 1999. He has expertise in the fields of nanoelectronic devices and advanced packaging.